jove

Three-dimensional Characterization of Interorganelle Contact Sites in Hepatocytes using Serial Section Electron Microscopy

Gary Hong Chun Chung[1], Paul Gissen[1,2], Christopher J. Stefan[1], Jemima J. Burden[1]

[1] MRC Laboratory for Molecular Cell Biology, University College London [2] NIHR Great Ormond Street Hospital Biomedical Research Centre, University College London

Corresponding Author

Jemima J. Burden

j.burden@ucl.ac.uk

Abstract

Transmission electron microscopy has been long considered to be the gold standard for the visualization of cellular ultrastructure. However, analysis is often limited to two dimensions, hampering the ability to fully describe the three-dimensional (3D) ultrastructure and functional relationship between organelles. Volume electron microscopy (vEM) describes a collection of techniques that enable the interrogation of cellular ultrastructure in 3D at mesoscale, microscale, and nanoscale resolutions.

This protocol provides an accessible and robust method to acquire vEM data using serial section transmission EM (TEM) and covers the technical aspects of sample processing through to digital 3D reconstruction in a single, straightforward workflow. To demonstrate the usefulness of this technique, the 3D ultrastructural relationship between the endoplasmic reticulum and mitochondria and their contact sites in liver hepatocytes is presented. Interorganelle contacts serve vital roles in the transfer of ions, lipids, nutrients, and other small molecules between organelles. However, despite their initial discovery in hepatocytes, there is still much to learn about their physical features, dynamics, and functions.

Interorganelle contacts can display a range of morphologies, varying in the proximity of the two organelles to one another (typically ~10-30 nm) and the extent of the contact site (from punctate contacts to larger 3D cisternal-like contacts). The examination of close contacts requires high-resolution imaging, and serial section TEM is well suited to visualize the 3D ultrastructural of interorganelle contacts during hepatocyte differentiation, as well as alterations in hepatocyte architecture associated with metabolic diseases.

Introduction

Since their invention in the 1930s, electron microscopes have allowed researchers to visualize the structural components of cells and tissues[1,2]. Most investigations have provided 2D information, as building 3D models requires painstaking serial section collection, manual photography, negative processing, manual tracing, and the creation and assembly of 3D models from sheets of glass, plastic, or Styrofoam[3,4]. Almost 70 years later, there have been considerable advances in numerous aspects of the process, from microscope performance, serial section collection, automated digital imaging, sophisticated software and hardware for 3D reconstruction, visualization, and analysis to alternative approaches for what is now collectively termed volume EM (vEM). These vEM techniques are generally considered to provide 3D ultrastructural information at nanometer resolutions across micron scales and encompass transmission electron microscopy (TEM) and newer scanning electron microscopy (SEM) techniques; see reviews[5,6,7,8].

For example, focused ion beam SEM (FIB-SEM) uses a focused ion beam inside an SEM to mill away the surface of the block between sequential SEM imaging scans of the block's surface, allowing the repeated automated milling/imaging of a sample and building up a 3D dataset for reconstruction[9,10]. In contrast, serial block face SEM (SBF-SEM) uses an ultramicrotome inside the SEM to remove material from the block face prior to imaging[11,12], while array tomography is a nondestructive process that requires the collection of serial sections, onto coverslips, wafers, or tape, prior to setting up an automated workflow of imaging the region of interest in sequential sections in the SEM to generate the 3D dataset[13]. Similar to array tomography, serial section TEM (ssTEM) requires physical sections to be collected ahead of imaging; however, these sections are collected on TEM grids and imaged in a TEM[14,15,16]. ssTEM can be extended by performing tilt tomography[17,18,19]. Serial tilt tomography provides the best resolution in *x*, *y,* and *z,* and while it has been used to reconstruct whole cells[20], it is reasonably challenging. This protocol focuses on the practical aspects of ssTEM as the most accessible vEM technique available to many EM labs who may not currently have access to specialized sectioning or vEM instruments but would benefit from generating 3D vEM data.

Serial ultramicrotomy for 3D reconstruction has previously been considered challenging. It was difficult to cut straight ribbons of even section thickness, be able to arrange and pick up ribbons of the correct size, in the correct order, onto grids with sufficient support, but without grid bars obscuring regions of interest, and most importantly, without losing sections, as an incomplete series may prevent full 3D reconstruction[21]. However, improvements to commercial ultramicrotomes, diamond cutting and trimming knives[22,23], electron lucent support films on grids[21,24], and adhesives for aiding section adhesion and ribbon preservation[13,21] are just some of the incremental advances over the years that have made the technique more routine in many labs. Once serial sections have been collected, serial imaging in TEM is straightforward and can provide EM images with subnanometer px sizes in *x* and *y,* allowing high-resolution interrogation of the subcellular structures-a potential requirement for many research questions. The case study presented here demonstrates the use of ssTEM and 3D reconstruction in the study of endoplasmic reticulum (ER)-

organelle contacts in liver hepatocytes, where ER-organelle contacts were first observed[25,26].

While being contiguous with the nuclear envelope, the ER also makes close contacts with numerous other cell organelles, including lysosomes, mitochondria, lipid droplets, and the plasma membrane[27]. ER-organelle contacts have been implicated in lipid metabolism[28], phosphoinositide and calcium signaling[29], autophagy regulation, and stress response[30,31]. The ER-organelle contacts and other interorganelle contacts are highly dynamic structures that respond to cellular metabolic needs and extracellular cues. They have been shown to vary morphologically in their size and shape and the distances between organelle membranes[32,33]. It is thought that these ultrastructural differences are likely to reflect their different protein/lipid compositions and function[34,35]. However, it is still a challenging task to define interorganelle contacts and analyze them[36]. Hence, a reliable yet simple protocol to examine and characterize interorganelle contacts is required for further investigations.

As ER-organelle contacts can range from 10 to 30 nm in membrane-to-membrane separation, the gold standard for identification has historically been TEM. Thin-section TEM has revealed specific subdomain localization for resident ER proteins at distinct membrane contacts[37]. Traditionally, this has revealed ER-organelle contacts with nm resolution but often only presented a 2D view of these interactions. However, vEM approaches reveal the ultrastructural presentation and context of these contact sites in 3D, enabling full reconstruction of contacts and more accurate classification of contacts (point vs. tubular vs. cisternal-like) and quantification[38,39]. In addition to being the first cell type where ER-organelle contacts were

observed[25,26], hepatocytes have an extensive system of other interorganelle contacts that serve vital roles in their architecture and physiology[28,40]. However, thorough morphological characterization of ER-organelle and other interorganelle contacts in hepatocytes is still lacking. Accordingly, how interorganelle contacts form and remodel during regeneration and repair is of particular relevance to hepatocyte biology and liver function.

Protocol

All animals were housed in accordance with the UK Home Office guidelines, and the tissue harvesting was carried out in accordance with the UK Animal (Scientific Procedures) Act 1986.

1. Specimen fixation and preparation

1. Dissect the liver tissue into appropriate size pieces, approximately 8 mm x 8 mm x 3 mm, and place the pieces in warm phosphate-buffered saline (PBS, 37 °C).

2. Inject room temperature (20-25 °C) fixative (1.5% glutaraldehyde in 1% sucrose, 0.1 M sodium cacodylate) into the liver pieces and transfer them from PBS to fixative for up to 20 min at room temperature. Always keep the tissue submerged in solutions to avoid drying.
   NOTE: Aldehydes are irritants that are corrosive and potentially carcinogenic. Sodium cacodylate is toxic if swallowed or inhaled. All fixatives must be handled while wearing appropriate personal protective equipment, and the experiment should be performed in a fume hood. Good fixation will result in a firmer tissue.

3. Set up the vibrating microtome with a blade, ice bath, and a cold PBS-filled buffer tray. Mount the first piece of fixed

liver tissue on a specimen holder with cyanoacrylate glue and transfer the block to the vibrating microtome.

4. Following the manufacturer's recommendations, approach the tissue and slice the fixed liver into 100 μm-thick slices.

5. Collect the slices using a spatula or natural hair paintbrush and transfer them into a 12- or 24-well dish containing ice-cold fix (1.5% glutaraldehyde, 0.1 M sodium cacodylate) on ice. Leave the slices on ice until all samples have been sliced and are ready to be processed further.

6. Select the slices containing the regions of interest for further processing and wash with gentle agitation. Perform three, 5 min washes with room temperature 0.1 M sodium cacodylate in a 12- or 24-well dish, ensuring the slices have sufficient buffer to move freely.

    NOTE: In general, regions of interest are selected based on anatomical features related to the biological question of the study and guided by regions of the tissue that are likely to be present in the entire series, e.g., not on the edge of the section, and that are well preserved.

7. In a fume hood, replace 0.1 M sodium cacodylate with freshly prepared 1% osmium tetroxide/1.5% potassium ferricyanide. Place the 12- or 24-well dish in a sealed container and transfer the container to a hazardous-chemicals fridge for 1 h.

    NOTE: Osmium is extremely hazardous in case of ingestion, inhalation, and skin contact. Potassium ferricyanide is an irritant and is harmful by inhalation and skin contact. Always handle using appropriate personal protective equipment, and perform the experiment in a fume hood.

8. In a fume hood, remove the osmium tetroxide/potassium ferricyanide to a dedicated osmium waste bottle, and wash the samples for 5 min with 0.1 M sodium cacodylate three times. Leave the samples in a sealed container overnight at 4 °C.

    NOTE: Potential pause point. Samples can be stored in 0.1 M sodium cacodylate in a sealed container at 4 °C for weeks with little detriment to preservation. Ensure that there is sufficient buffer to prevent drying.

9. Incubate the samples with freshly prepared 1% tannic acid in 0.05 M sodium cacodylate for 45 min in the dark at room temperature.

    NOTE: Tannic acid is an irritant and can cause eye damage. Wear appropriate personal protective equipment and perform the experiment in a fume hood.

10. Perform three 5 min washes with ddH$_2$O prior to dehydration and embedding.

2. Sample dehydration, Epon resin embedding, and mounting

1. Prepare Epon resin according to the following ratio by weight (see step 2.2). Tare a balance with a 100 mL disposable plastic beaker containing a stir bar. Cut the ends from 5 disposable plastic Pasteur pipettes and use these to transfer viscous resin components into the beaker.

2. Sequentially add 19.2 g of resin-812, 7.6 g of DDSA, 13.2 g of MNA, and 0.8 g of DMP-30 accelerator into the beaker. Using the fifth clean plastic Pasteur pipette, thoroughly mix the resin components by hand.

    NOTE: Avoid introducing bubbles but ensure sufficient mixing of the bottom resin with the top to achieve a color change and rough mixing of the component layers.

All resin components are irritants and are harmful by inhalation and skin contact. DMP-30 is corrosive and can cause skin corrosion. Wear appropriate personal protective equipment.

3. Place the beaker on a magnetic stirrer and leave to stir gently, periodically mixing the resin manually.

4. Wash the samples with gentle agitation for 5 min with 70% ethanol; repeat once.

5. Wash the samples with gentle agitation for 5 min with 90% ethanol; repeat once.

6. Wash the samples with gentle agitation for 5 min with 100% ethanol; repeat once.

7. While the samples are in 100% ethanol washes in a fume hood, prepare a 50:50 (v/v) propylene oxide (PO):Epon mixture in a glass vial with a propylene oxide (PO)-resistant plastic lid. Carefully but securely clip on the glass vial lid, and while keeping hold of both lid and vial, shake or vortex to mix.

   NOTE: Propylene oxide is an acutely toxic, flammable irritant that dissolves some plastics. Wear appropriate personal protective equipment and perform the experiment in a fume hood.

8. After step 2.6, incubate the samples with PO:Epon for 1 h in a PO-resistant container (e.g., aluminum trays or glass vials), with gentle rocking/agitation in the fume hood.

9. In the fume hood, transfer the samples to 100% Epon. Incubate for 2 h at room temperature in the fume hood with rocking/rotation/agitation. Transfer the PO:Epon mixture to a dedicated glass Epon waste bottle.

10. Repeat step 2.9 once.

11. Mount the samples for embedding. Depending on the size of the slices and the region of interest, directly mount the slices onto prepolymerized resin stubs or flat-embed them for dissection and re-embed them at a later date.

    NOTE: For flat-embedding, a "cast-a slide" can be used to embed many slices at once. Leftover resin can be used to fill beam capsules and baked to make prepolymerized stubs or frozen for later use.

12. Once mounted and covered in sufficient resin to fill the "cast-a slide" cavity, bake the samples overnight in a 60 °C oven.

    NOTE: Potential pause point. Samples can be stored at room temperature for years.

13. For re-embedding, identify the region of interest in the flat embedded tissue slices. Using a jeweler's saw, cut out the piece of tissue of appropriate size ($1 \ mm^2$ to $4 \ mm^2$) and re-embed using resin prepared, as in step 2.2, onto the top of a prepolymerized block and bake overnight in a 60 °C oven.

    NOTE: Alternatively, the tissue piece can be glued to a stub or pin with two-part epoxy resin. Leave to set overnight. Potential pause point.

3. Trimming and serial sectioning of embedded samples

NOTE: Sectioning is a learned skill; users should be proficient at ultrathin sectioning prior to attempting serial sectioning. As exact microtome controls vary across manufacturers, follow the manufacturer's instructions and guidelines.

1. With the sample locked in the trimming adaptor, use a razor blade to carefully trim the resin embedded tissue to meet the following criteria (see **Figure 1A,B**):

   1. Ensure there is a flat, top surface exposing the tissue around the region of interest.

2. Ensure a trapezoid shape with the top and bottom edges being clean and parallel.

3. Ensure overall dimensions of 200-500 μm in *x*, 100-500 μm in *y*.

4. Ensure an asymmetric block face, e.g.*,* right-hand side corners of ~90 °, top left corner obtuse, and left-hand bottom corner acute.

NOTE: A trimming cryoknife can be an alternative tool for a razor blade. The other recommendations are for user convenience for ordering sections when imaging. Optional: If sections fail to form stable ribbons, a contact cement can be applied to the leading edge of the block face to aid ribbon formation. Razor blades are sharp; take care to hold the razor blade such that accidental slippages are unlikely to result in personal harm.
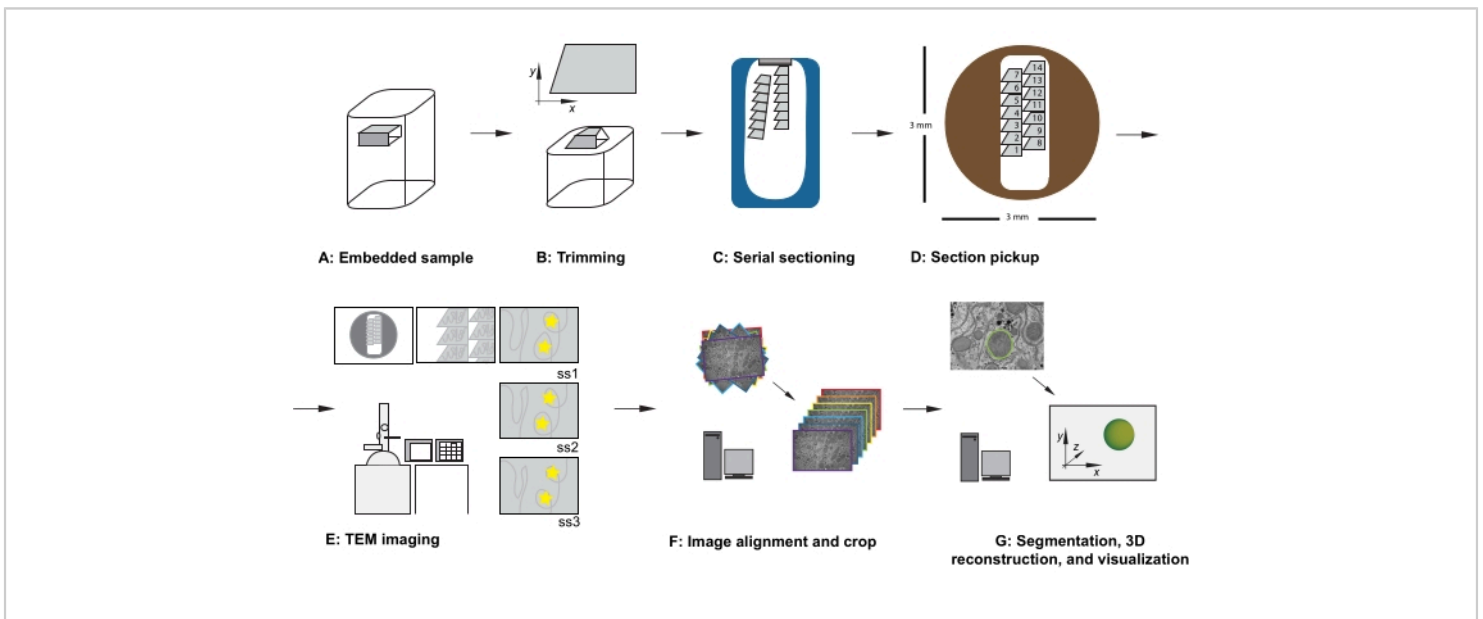

Figure 1: Serial section TEM workflow. (A) Diagram of the specimen in the resin block. (**B**) Trim block to generate a trapezoid shape with edges suitable for serial sectioning and asymmetric block face to ensure known orientation. (**C**) Diagram showing ribbons of serial sections, floating on the water's surface in the diamond knife boat. (**D**) Diagram showing the section and ribbon organization, dictating order of sections, on a 3 mm diameter TEM slot grid. (**E**) TEM imaging and navigation. Showing ribbon and section order and using "yellow star stickers" on the monitor for screen referencing to ensure reimaging of the same region of interest in subsequent sections. (**F**) Image alignment and cropping. (**G**) Segmentation, 3D reconstruction, and visualization. Abbreviation: TEM = transmission electron microscopy. Please click here to view a larger version of this figure.

2. Once trimmed, transfer the specimen arc, together with the chuck and the sample, to the specimen arm of the microtome, positioning the specimen arc so that the arc's travel range runs from top to bottom; secure the specimen arc in place.

3. Place and lock the diamond knife in the knife holder, ensuring that the cutting angle is set appropriately to the knife. Lock the knife holder into the stage securely.

4. With the stage uplighting on, use the knife advance while constantly checking the relationship between the block face and the knife's edge. Cautiously advance the knife towards the specimen, continually adjusting the knife's lateral angle, specimen tilt, and specimen rotation by adjusting the relevant knobs until the block is aligned to the knife's edge.

5. Turn off the stage uplighting; turn on the stage downlighting; set the top and bottom of the cutting window of the specimen arm; and leave the specimen just below the knife edge.

6. Fill the knife boat with clean ddH$_2$O and ensure the water surface is level with the knife's edge and just slightly concave.

7. Optional: Dip an eyelash into the 0.1% Triton X-100 and then in the knife boat water to reduce the surface tension of the water to aid chloroforming and ribbon pickup.

8. Prepare the workstation with eyelashes (eyelash glued to a cocktail stick), formvar-coated slot grids, labeled crossover forceps, chloroform, 0.1% Triton X-100 solution, distilled water, filter paper, and grid box with grid box notes.

9. Set the cutting speed at 1 mm/s and the initial cutting thickness to 100 nm and start the cutting cycle.

10. After the first section is cut, change the cutting parameters to a cutting speed at 0.8 mm/s and the cutting thickness to 70 nm, and continue cutting, allowing sections to form a ribbon moving down the surface of the water-filled knife boat (**Figure 1C**).

NOTE: It is important to be aware of the color of the sections being produced as this is often a more accurate guide to the thickness of the resin sections. Silver sections are usually around 70 nm thick, while grey sections are thinner and gold sections are thicker.

11. Allow the microtome to continue cutting sections and the ribbon to get longer.

NOTE: It is important to avoid large vibrations and physical disturbances in the room. Drafts can cause the sections to move on the surface of the water in the knife boat, and physical vibrations can cause the microtome to cut unevenly.

12. Once enough sections are collected and before the ribbon gets to the end of the boat, stop the cutting (just after the sample has passed the knife's edge).

NOTE: The number of sections needed depends on the size of the block face and the size of the dataset to be collected. Thus, it is useful to be aware of the relationship between the size of the block and the slot grid as the cut sections are coming off.

13. Using an eyelash in each hand, gently break the ribbon into smaller ribbons that can fit in the length of the slot grid, taking care to make a note of their relative positions from within the sample.

NOTE: If their combined width fits, multiple ribbons can be gently placed next to each other and picked up together in a single slot grid. If picking up multiple ribbons on a single slot grid, pay attention to the order and the relative position of the ribbons. For example, always place the ribbons further into the sample to the right of a ribbon already in the sample (**Figure 1D**).

14. Optional: Using a glass applicator rod, hover a drop of chloroform over the sections to flatten them out.

NOTE: Chloroform is toxic and an irritant. Do not let chloroform touch the water surface or sections. If it accidentally does, the water needs to be removed and the knife washed before returning to sectioning. The chloroform can damage the sections and degrade the glue that secures the diamond into the knife boat.

15. Using the first numbered forceps, pick up the first empty slot grid (on the right-hand side of the slot, formvar side down), gently dip in the Triton X-100, and then twice in the distilled water before removing excess water from the forceps edge using a piece of filter paper.

16. With an eyelash in one hand and the forceps in the other hand, gently lower approximately 2/3rd of the formvar-coated slot grid into the water of the knife boat (away from the sections), so that the formvar side is facing down, and the right-hand long edge of the slot is at the surface of the water and parallel to the water's edge.

17. Gently waft the grid in the water towards the ribbons so that upon the return stroke, the sections drift towards the grid. Continue to do this in smaller and smaller wafts until the right-hand edge of the ribbon lines up with the right-hand edge of the slot. Then, with the last waft, gently bring the grid up to pick the sections up into the slot grid.

18. Leave the grid in the forceps to dry before storing it in the grid box, appropriately annotated on the grid box reference sheet.

19. Repeat step 3.16 until all ribbons are collected, ensuring that the order of ribbons is maintained.

20. If further sections are required, retract the knife 150 nm or so, check the water level in the boat, and add more if required. Start the cutting process again, following steps 3.11-3.18.

21. Once all sections are collected, ensure the knife edge is free from section debris, retract the knife away from the block face, and remove and clean the knife.

4. Grid staining

1. Once dry, stain the sections with Reynolds' lead citrate either on parafilm on the bench or in a Petri dish. Place several pellets of sodium hydroxide under a Petri dish lid to provide a carbon dioxide-free environment. Then, carefully, away from the pellets, pipette 40 µL drops of Reynolds' lead citrate on the parafilm, one for each grid. **NOTE:** Do not stain too many grids at once; e.g., the maximum should be 6. Try not to breathe directly on the staining dish. Carbon dioxide can react with the lead citrate and cause unwanted precipitate on the grids.

2. Invert each grid (section side down) onto the lead citrate drop and leave protected by the Petri dish lid for 7 to 10 min. While the grids are staining, prepare a larger second piece of parafilm on the bench with five 300 µL drops of distilled water for each grid.

3. At the end of the lead citrate incubation, transfer each grid to a droplet of distilled water to wash for 1 min without breathing directly on the grids.

4. Repeat step 4.3 a total of five times.

5. Using numbered crossover forceps, pick up the first grid, touch the edge of the grid to filter paper to wick away most of the water, and allow to dry in the forceps (for at least 20 min). Repeat for each grid.

5. Imaging acquisition by TEM

NOTE: As exact TEM controls vary across manufacturers, follow the manufacturer's instructions and guidelines. The

following steps should be performed by users who are already proficient at TEM use.

1. Prior to imaging, perform the usual checks, e.g., beam alignment, gain references, and sample eucentricity.

2. Carefully load the first grid of serial sections into the specimen holder, taking care to align the slot (and therefore sections) to the vertical axis of the microscope stage.
   NOTE: This accuracy is not essential but saves time during acquisition and future data handling stages. When inserting the grid (section side down or section side up), take care to image all grids in the same orientation.

3. At low magnification, observe the order, location, and position of the serial sections (**Figure 1E**). Navigate to the middle section of the series on the grid.
   NOTE: Depending on the exact research aim, approaches for imaging may vary; however, the following is a useful starting point. The shape of the sections and the relationship of the ribbons (as picked up in step 3.14) dictate which section was first and which section was last on the grid.

4. Browse the sample and identify a region of interest. Observe the sample at the desired magnification, and consider collecting the series at a slightly lower magnification, as sections are often not perfectly aligned, and images may need to be cropped later.

5. Take reference images at lower magnifications to appreciate the context of the region of interest, its rough location at different magnifications in relation to section boundaries, and landmark features within the sample.

Use these to sign-post the region of interest in other sections.

6. Optional: for screen referencing, use reusable adhesive putty, stickers, or a piece of overhead projector (OHP) paper, taped to the screen, to place temporary markers on the screen to allow routine reimaging of the same features of the region of interest in the center of the image, throughout the dataset (see yellow stars in **Figure 1E**).

7. Using the reference images, navigate to the region of interest on the first section of the grid, and acquire an image at the desired magnification.
   NOTE: When saving images, note down the first file name of the first image of the series, and use sequential naming nomenclature so that all image names follow the sequential order of the serial sections.

8. Navigate to the next section and repeat step 5.7 until all sections have been imaged for that region of interest.

6. Image export and serial section alignment registration

1. Export the image files belonging to the same stack into a single folder. Make sure the folder is sorted by file name.
   NOTE: The images should ideally have the same root name and follow the order in which they have been acquired.

2. Open Fiji and click on **File | Import | Image Sequence**.

3. Click on the first image of the folder and click **Open**. Wait for a popup window of **Sequence Options** to appear (**Figure 2A**).
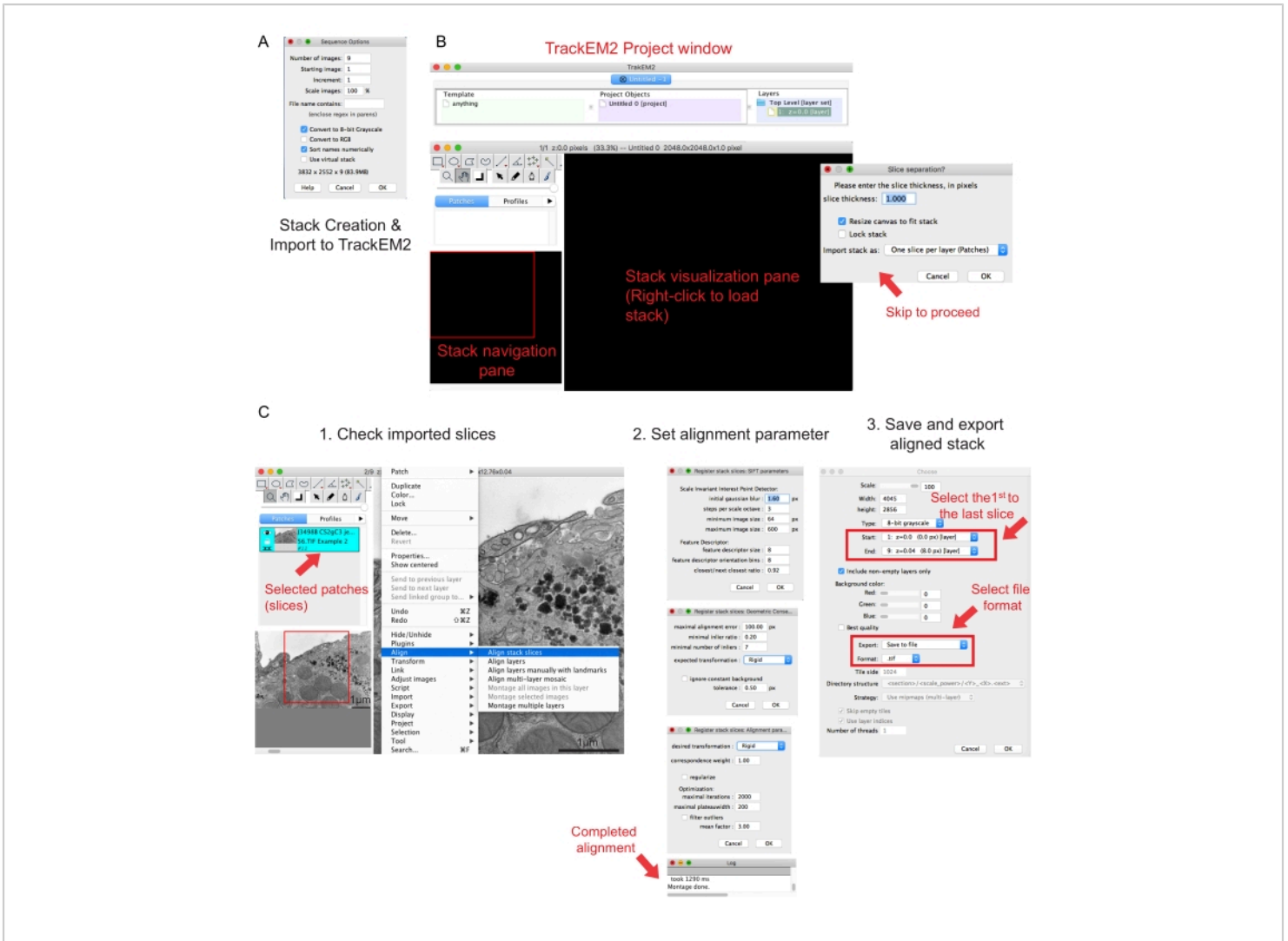
Figure 2: Creation of a serial stack and serial section alignment using Fiji. (**A**) Screenshot showing the Sequence Options when loading the images for making a serial stack. (**B**) Screenshot of the TrackEM2 plugin and the key windows of the plugin. Press **OK** in the Slice separation to proceed with the alignment. (**C**) Screenshot after successfully loading the serial stack into the visualization pane. Three sequential windows of alignment parameters will pop up once **Align stack slices** are selected. Export the aligned stack once the alignment is completed. Please click here to view a larger version of this figure.

4. Click **Sort names numerically | Convert to 8-bit** option. Press **OK**.

   NOTE: Conversion to 8-bit aids import of the data into Amira and reduces the file size, allowing quicker processing speeds in later steps.

5. Check the completeness, sequence, and magnification of the created stack. Save the created stack as a .tif file.

   NOTE: Images should have been acquired at the same magnification.

6. Execute the TrakEM2 plugin[41]. Go to **File | New | TrackEM2 (blank).**

   NOTE: The plugin will ask the user to save the TrackEM2 files. If needed, save the TrackEM2 files to the image folder. Three windows should appear: a project window, a stack navigation (left) window, and a stack visualization pane (**Figure 2B**).

7. Right-click to the black visualization pane. Click **Import | Import stack** and select the previously created stack.

8. Click **OK** to load the stack to the stack navigation window.

   NOTE: A Slice separation window will pop up to ask for pixel and dimension relationship. For only stack alignment, click **OK** to skip this step.

9. Use the slider to check all the slices of the stack. Look for the loaded slice, which will appear as a patch in the navigation plan. Select the patches that will be included in the following alignment.

   NOTE: Selected patches will go blue.

10. Hover the mouse over the viewing pane. Right-click the image, select **Align | Align stack slices** (**Figure 2C-1**).

11. Specify the alignment parameters through a set of three sequential windows.

    NOTE: For most data, start with a rigid alignment (allows for rotation and translation but not transformation) and keep other parameters as default (**Figure 2C-2**).

12. Allow the alignment to run until the readout log says **Montage done**.

    NOTE: Runtime depends on the number of voxels and the speed of the computer.

13. Check the aligned stack in the viewing pane. Press **Alt** and **-** keys (in PC) or the **Ctrl** and **-** keys (in Mac) for a zoom-out view of the aligned stack.

14. If satisfied with the aligned stack, right-click **Export | Make flat image** to save the aligned stack.

15. Select the first image as the start of the stack and the last image as the end of the stack, click **OK** (**Figure 2C-3**). Save the aligned stack as .tif.

    NOTE: To reduce file size, crop the data to only contain the necessary region of interest.

16. If needed, execute an affine alignment on the aligned stack. Open the aligned stack in Fiji, select **Plugin | Registration | StackReg**.

17. Choose the **affine** option and press **OK**. Wait until the program is complete.

18. Save the affine-aligned stack with a different file name.

7. Segmentation and 3D reconstruction

1. Open Amira[42]. Click **File | Open Data** to load the aligned stack.

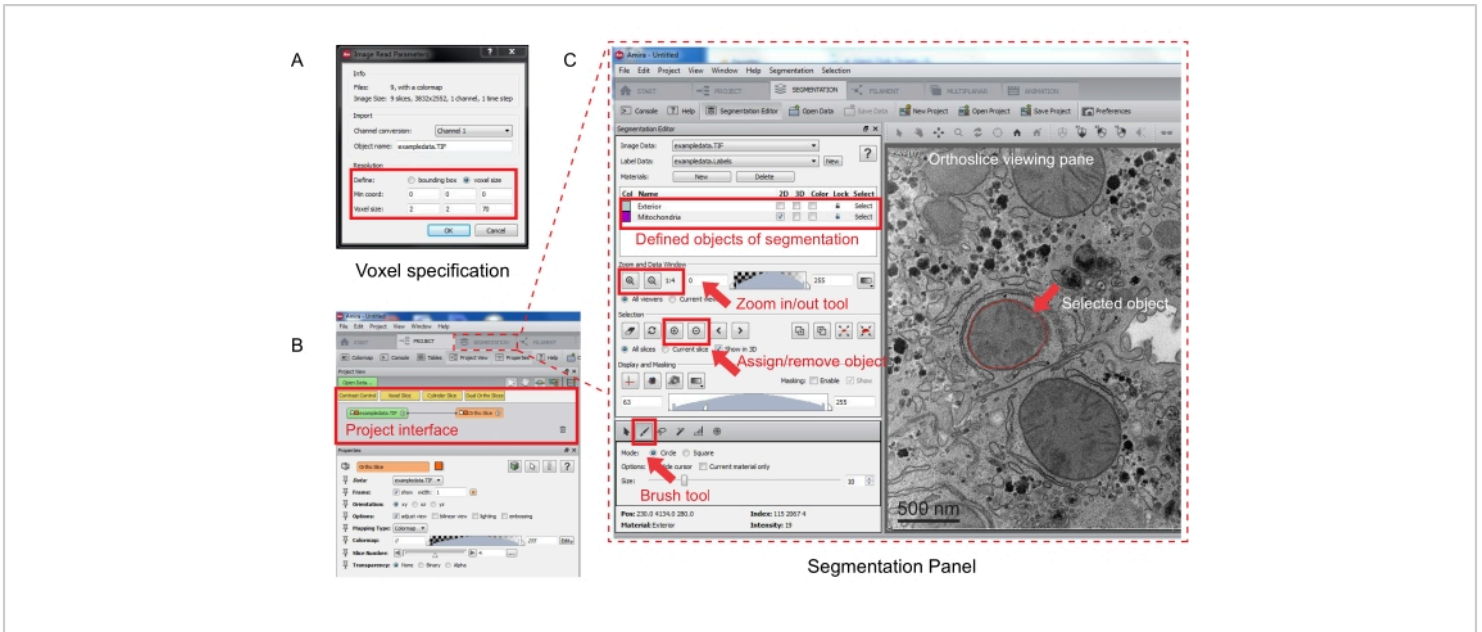2. Specify the voxel measurements in the new popup window (**Figure 3A**).

Figure 3: Segmentation of serial stack using Amira. (**A**) The Voxel definition popup window prior to loading an aligned stack. (**B**) Screenshot of the project interface after the import of a stack. Select the **Segmentation tab** to start object tracing in the **Segmentation Editor** panel. (**C**) Key features of the segmentation tab. Define the objects for segmentation in the **Segmentation Editor** section of the **Segmentation tab**. Use the **zoom** function to assist identification of objects. Select the **Brush** tool and trace the boundary of the object. Click the **+** symbol under **Selection** to assign the trace. An assigned object will appear to have a red boundary in the orthoslice viewing pane. Please click here to view a larger version of this figure.

NOTE: An image stack node will appear in the project interface, and an orthoslice will appear in the viewing pane on the right (**Figure 3B**).

3. To start segmentation, select the **Segmentation Tab** (**Figure 3B**).

    NOTE: It is recommended to save the segmentation progress before and during the segmentation. Go to **Model | Save Model As** any .am file that suits.

4. Click **New** in the segmentation editor panel to define new objects in the material list. Right-click to change the color of the object and double-click to rename the object.

5. For manual segmentation, choose the **segmentation** tool below the material list. Select the default **Brush** tool to highlight the pixels (**Figure 3C**).

    NOTE: Alternatively, use the **brush** tool to trace the outline of the object and press **Shift + F** to fill the object.

6. To convert the **brush** tool into an **eraser**, continually press **Ctrl** while selecting pixels for correction. Annotate every slice in the stack.

7. Once confirmed, assign the selection to a label by clicking the **+** sign. Click the **-** sign to remove the selection.

8. Go back to the project interface once the segmentation is complete. Look for a node with a ".label" extension connected to the image stack.

9. Right-click the ".label" extension and select **Generate Surface | Apply** to create a .surf file.

10. To render the 3D model of a segmented object, right-click the .surf file and select **Surface view** to generate a 3D model in the viewing pane.

11. Save the 3D model for visualization or further quantitative analyses.

Representative Results

For this technique, regions of interest are selected based on the biological research aim and identified prior to the trimming and sectioning of embedded tissue. Similarly, the size of the block face may be dictated by the research question; in this case, the sample was trimmed to leave a block face of approximately 0.3 mm x 0.15 mm (**Figure 4A**). This allowed for two grids of 9 serial sections per grid, providing 18 serial sections and incorporating a volume of liver tissue of a volume of approximately 62 μm^3 (316 μm x 150 μm x 1.3 μm). This volume was sufficient to allow the complete 3D reconstruction of individual mitochondria in liver tissue.
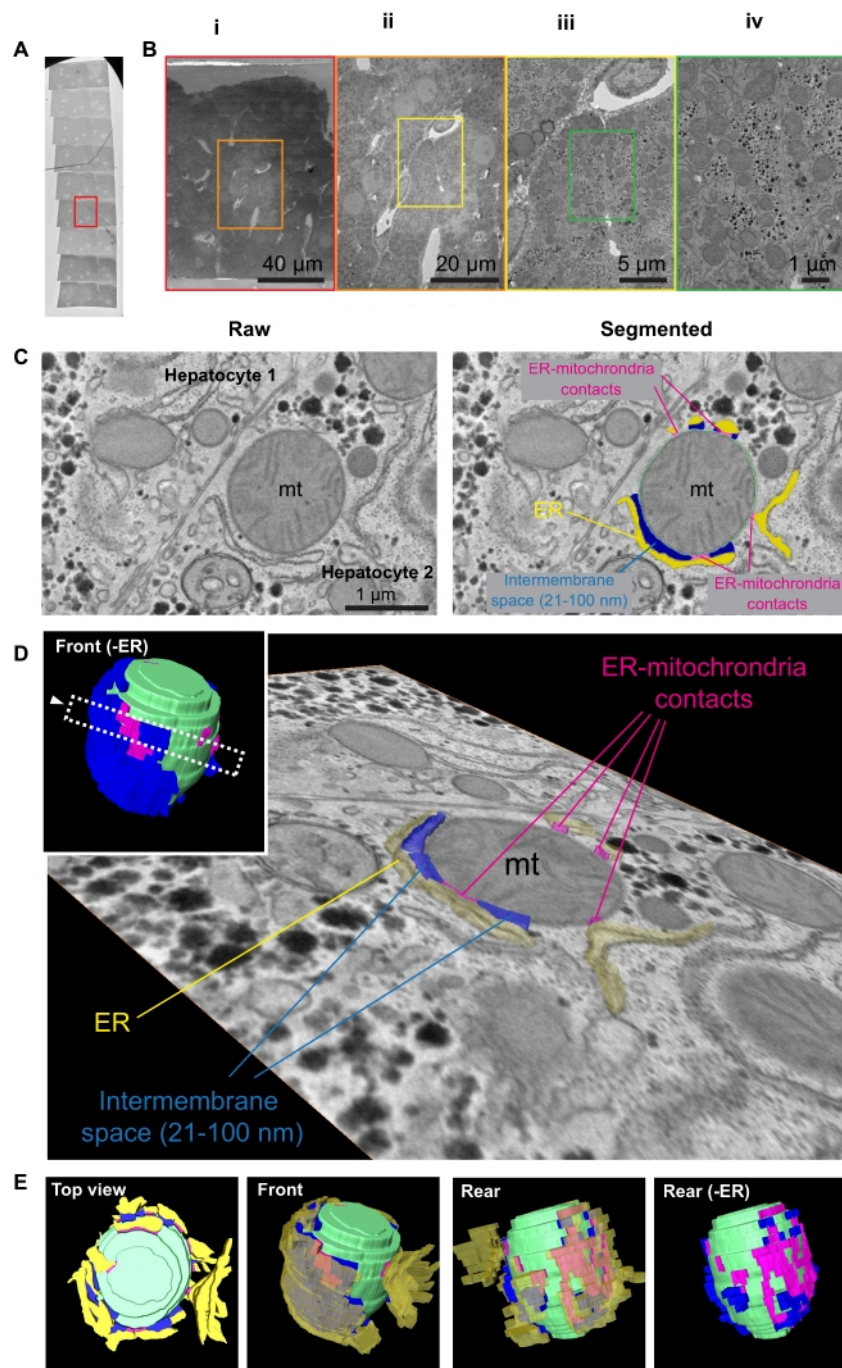
Figure 4: Segmentation and 3D reconstruction reviewing the morphology of ER and associated ER-mitochondria contacts. (**A**) Overview of ribbon of serial sections in the TEM. (**B**) Low-magnification view of region of interest and contextual landmarks for relocation. Scale bars = 40 µm (i), 20 µm (ii), 5 µm (iii), 1 µm (iv). (**C**) Left: EM tomogram of two apposed hepatocytes. Right: segmented version of the same tomogram. Trace of the ER (yellow), mitochondria (cyan), and intermembrane contacts between the ER and mitochondria of different space: 0-20 nm (magenta); 21-100 nm (blue). (**D**) An

orthoslice isolated from the reconstructed model showing only the ER and the different membrane contacts, corresponding to the arrow annotated region in the inset. (**E**) 3D reconstruction of the segmented organelles and ER-mitochondria contacts at different angles. Abbreviations: ER = endoplasmic reticulum; TEM = transmission electron microscopy; mt = mitochondria. Please click here to view a larger version of this figure.

Visualization of the serial sections by TEM at low magnification helps to identify the designated area of interest and its context within the rest of the tissue (**Figure 4B**). These images can be used to find the same region of interest in subsequent sections. A region of interest showing good preservation at a boundary between two apposed hepatocytes was selected and presented here. Higher magnification imaging allows the observation of the morphological details of the different organelles (**Figure 4C**) with nm resolution. To illustrate two types of ER-organelle associations, selected mitochondria and the ER were segmented, manually tracing the edge of the membranes presenting with enhanced electron density. Afterward, the brush tool was set to a fixed nm/px thickness (**Figure 3B**) and used to follow the boundary of the organelle of interest to highlight the regions between the two targeted organelles that were within a specified contact distance to one another and could be designated as a particular class of organelle contacts. **Figure 4D** shows a tilted orthoslice overlaid with segmentation traces and its relative position (arrowhead in the inlet 3D model) within the whole mitochondrion.

The traces were assigned different colors, reconstructed into a 3D model after segmentation, and displayed at different orientations (**Figure 4E**). The ER (yellow) structure was shown to be partially transparent in the middle panels to visualize the ER-mitochondria contacts and mitochondria (cyan) underneath. The front and rear views of the model reveal an asymmetrical distribution of interorganelle contacts of different intermembrane spacings. Intermembrane space

smaller than 21 nm was assigned as ER-mitochondria contact (pink) because functions such as lipid transfer have been reported to be feasible at this distance[43]. The intermembrane space (blue) between 21 and 100 nm was also annotated because this region may represent the recently reported mitochondria-rough-ER associations[44]. Wrapping ER structures of similar curvature were observed in the 3D model (**Figure 4E**). **Figure 4D** shows an example of changing intermembrane distance (~40 nm → ~20 nm → ~40 nm) between the wrapping ER cisternae and the mitochondria. The method allows follow-up patch analysis of these two distinct intermembrane spaces, such that quantitative analysis of their abundance, distribution, and topology is possible.

Concerns	Serial Tomography	Serial Section TEM	FIB-SEM	SBF-SEM	Array Tomography
Lateral *(x,y)* resolution (Minimum px size)	0.5 nm	0.5 nm	2 nm	2 nm	2 nm
Axial *(z)* resolution (Minimum px depth)	1 nm	50 nm — Limited to section thickness	4 nm	20 nm	50 nm — Limited to section thickness
Volume ranges of data in typical applications	0.1 - 50 µm^3	10 - 250 µm^3	10 - 1 x 10^4 µm^3	10 – 1 x 10^{12} µm^3	10 - ∞ µm^3
Revisit or reimage of the samples	Possible	Possible	Not possible	Not possible	Possible
Cost of the equipment (instrument examples)	££ (200 kV TEM)	£ (120 kV TEM)	££ (FIB-SEM)	££ (SBF-SEM)	££ (SEM+AT)
Cost of equipment maintenance	££	£	££	££	£

Table 1: Overview of volume electron microscopy techniques. Abbreviations: EM = electron microscopy; TEM = transmission EM; FIB-SEM = focused ion beam SEM; SBF-SEM = serial block face SEM; SEM + AT = SEM with Array Tomography.

Discussion

An accessible vEM technique for visualizing organelle structure and interactions in 3D is described in this protocol. The morphology of interorganelle contacts in hepatocytes is presented as a case study here. However, this approach has also been applied to investigate a variety of other samples and research areas, including Schwann cell-endothelial interactions in peripheral nerves[45], Weibel Palade Body biogenesis in endothelial cells[46], cargo secretion in kidney cells[47], and synapse morphology in hippocampal neurons[48]. To better understand liver biology, this approach can be used to investigate hepatocyte morphology in 2D cell culture, 3D hepatic organoid model systems[49], and liver

tissue. This robust and flexible approach can be used by many laboratories with access to a conventional 120 kV transmission electron microscope and ultramicrotome and does not require expensive sample preparation techniques.

While this is an accessible protocol, it is important to note that there are alternative vEM techniques that can provide certain advantages to the researcher, depending on the research question; see **Table 1** for an overview[6,50,51]. Often the resolution and volume of the data needed directly influence the researchers' choice of the vEM technique and the ease and speed at which the project can progress. FIB-SEM, for example, can remove very thin layers from the sample prior to imaging, resulting in excellent z-resolution (*z* thickness

as low as 4 nm) and potentially providing volumetric 3D data with isotropic voxels. This allows visualization of the data with equal resolution from every angle, which can sometimes provide distinct advantages when contact points are difficult to discern[52,53]. FIB-SEM can generate large volumes but is often costly and time-consuming, while SBF-SEM is an excellent technique to use when larger volumes are required, e.g., 100s to 1000s of sections[54]. SBF-SEM and array tomography provide similar *xy* resolution as FIB-SEM but with reduced z-resolution. As array tomography involves collecting physical sections, the z-resolution is perhaps the poorest of its competitors (*z* thickness 50+ nm) but has several distinct advantages. Foremost, because it is a nondestructive technique, the sample can be revisited at different *xy* resolutions, with easy montaging, at various times, and across numerous regions, allowing full context and detail to be appreciated in a single sample. Serial section TEM also shares this benefit; however, as sections need to be collected onto TEM grids, it is better suited to smaller volumes that require fewer sections to be collected prior to imaging. However, it is compatible with TEM tilt tomography, a technique that provides very high *z*-resolution (*z* thickness as low as 2 nm) of very small volumes, enabling further interrogation of specific contact sites of interest if required.

Regardless of the vEM approach taken, sample preservation is critical to the success of the project. The fixation medium should be an isotonic match to the tissues, and the transfer to the fixation medium should be done rapidly to avoid drying of the tissues[55]. Liver tissue can be challenging to preserve, and while it offers excellent preservation, allowing retention of liver tissue for additional experiments, whole liver perfusion for electron microscopy is often not possible. Liver-wedge needle perfusion is an excellent alternative[56]. Cryoimmobilization is also an option but requires immediate high-pressure freezing to achieve homogeneous vitrification of fresh vibratome sections; thus, this approach is quite challenging. After initial fixation, there are a variety of EM specimen preparation protocols that yield satisfactory results. A routine TEM protocol is presented here[57], but "enbloc megametal" protocols have also been successfully employed with other biological samples[45,58]. While these "enbloc megametal" protocols provide more contrast in the sample, giving some structures a more heavily stained appearance, they also have the advantage of removing the requirement to stain sections, thus reducing the risk of adding unwanted stain precipitate on samples and damaging grids in the process.

Another critical step in this protocol is ultrathin sectioning and ribbon collection. Collecting serial sections from the water surface of the cutting boat is a manual process that could lead to damaged and missing sections. For example, should sections fail to adhere to each other and form stable ribbons, contact cement can be applied to the leading edge of the blockface to stabilize the ribbons[13]. The duration and routine success of this step are skill-dependent[59]. Although a plethora of model-specific section-picking methods[60,61] may confuse beginners, some simple, practical guides[55,62] for routine sectioning, together with practice, can significantly improve sectioning skills. This protocol requires minimal specialist equipment, and with the aid of video footage showing the practical aspects of manual manipulation techniques during sectioning, ribbon detachment, and ribbon handling and pickup, provides an excellent beginner's guide to serial sectioning.

Volume EM image analysis continues to be an area of development with a variety of open-source and commercial software options currently available, and the list is ever-growing. A selection of software for alignment (TrakEM2[41]),

JOVE

3D segmentation, and reconstruction (Amira[42]) are presented here; however, many alternatives are available for alignment (e.g., Fiji, Register Virtual Slices[63], Atlas5, and 3D reconstruction (e.g., MIB[64]; Reconstruct[65]; IMOD[66]). For relatively small analysis projects, regardless of whether the data are generated locally or sourced from openly shared datastores (EMPIAR[67], Open Organelle[68]), manual segmentation described here is an accessible and feasible option. However, for larger datasets, many users are turning to machine learning and artificial intelligence for automation of these tasks[69,70], as well as crowd-sourcing volunteers[71] or combining both[72].

Ultimately, after alignment and 3D segmentation, 3D reconstruction reveals not only the morphology of the structures in question but, importantly, also their relationship with other organelles, including the unique characteristics of any contact sites present. These organelle contacts can be analyzed further, and features such as the number of contacts, contact area, volumes of organelles, and morphometric parameters of the organelles can be extracted and compared between experimental models[70]. Quantitation options are numerous, and their relevance varies hugely depending upon the exact research question. Hence, they have not been covered in depth as part of this protocol.

Pathological processes affecting organelle contacts have been implicated in both the rare (e.g., Wilson's disease) and common (viral hepatitis and non alcoholic steatohepatitis) disorders[73,74,75]. For example, the ER-mitochondria and mitochondria-lipid droplet contact sites appear to regulate lipid metabolism in hepatocytes; therefore, the study of these contacts is of great interest. In conclusion, serial section TEM and subsequent 3D reconstruction and analysis is a powerful technique to interrogate interorganelle contacts and probe their relative importance in liver functions and diseases.

Disclosures

The authors have no conflicts of interest to disclose.

Acknowledgments

References

1. Knoll, M., Ruska, E. Das elektronenmikroskop. *Zeitschrift für Physik.* **78** (5), 318-339 (1932).

2. von Ardenne, M. Das elektronen-rastermikroskop. *Zeitschrift für Physik.* **109** (9), 553-572 (1938).

3. Bang, B. H., Bang, F. B. Graphic reconstruction of the third dimension from serial electron microphotographs. *Journal of Ultrastructure Research.* **1** (2), 138-139 (1957).

4. Birch-Andersen, A. Reconstruction of the nuclear sites of Salmonella typhimurium from electron micrographs of serial sections. *Journal of General Microbiology.* **13** (2), 327-329 (1955).

5. Denk, W., Horstmann, H. Serial block-face scanning electron microscopy to reconstruct three-dimensional tissue nanostructure. *PLoS Biology.* **2** (11), e329 (2004).

6. Peddie, C. J., Collinson, L. M. Exploring the third dimension: volume electron microscopy comes of age. *Micron.* **61**, 9-19 (2014).

7. Titze, B., Genoud, C. Volume scanning electron microscopy for imaging biological ultrastructure. *Biology of the Cell.* **108** (11), 307-323 (2016).

8. Kornfeld, J., Denk, W. Progress and remaining challenges in high-throughput volume electron microscopy. *Current Opinion in Neurobiology.* **50**, 261-267 (2018).

9. Heymann, J. A. et al. Site-specific 3D imaging of cells and tissues with a dual beam microscope. *Journal of Structural Biology.* **155** (1), 63-73 (2006).

10. Knott, G., Marchman, H., Wall, D., Lich, B. Serial section scanning electron microscopy of adult brain tissue using focused ion beam milling. *Journal of Neuroscience.* **28** (12), 2959-2964 (2008).

11. Leighton, S. B. SEM images of block faces, cut by a miniature microtome within the SEM - a technical note. *Scanning Electron Microscopy.* (Pt 2), 73-76 (1981).

12. Martone, M. E., Deerinck, T. J., Yamada, N., Bushong, E., Ellisman, M. H. Correlated 3D light and electron microscopy: use of high voltage electron microscopy and electron tomography for imaging large biological structures. *Journal of Histotechnology.* **23** (3), 261-270 (2000).

13. Micheva, K. D., Smith, S. J. Array tomography: a new tool for imaging the molecular architecture and ultrastructure of neural circuits. *Neuron.* **55** (1), 25-36 (2007).

14. Sjostrand, F. S. Ultrastructure of retinal rod synapses of the guinea pig eye as revealed by three-dimensional reconstructions from serial sections. *Journal of Ultrastructure Research.* **2** (1), 122-170 (1958).

15. Ware, R. W. Three-dimensional reconstruction from serial sections. *International Review of Cytology.* **40**, 325-440 (1975).

16. Stevens, J. K., Davis, T. L., Friedman, N., Sterling, P. A systematic approach to reconstructing microcircuitry by electron microscopy of serial sections. *Cognitive Brain Research.* **2** (3), 265-293 (1980).

17. Hoppe, W. Three-dimensional electron microscopy. *Annual Review of Biophysics.* **10**, 563-592 (1981).

18. Frank, J. *Electron tomography: methods for three-dimensional visualization of structures in the cell.* Springer, New York, NY (2008).

19. Baumeister, W. Electron tomography: towards visualizing the molecular organization of the cytoplasm. *Current Opinion in Structural Biology.* **12** (5), 679-684 (2002).

20. Hoog, J. L., Schwartz, C., Noon, A. T., O'Toole, E. T. Organization of interphase microtubules in fission yeast analyzed by electron tomography. *Developmental Cell.* **12** (3), 349-361 (2007).

21. Harris, K. M., Perry, E., Bourne, J., Feinberg, M., Ostroff, L., Hurlburt, J. Uniform serial sectioning for transmission electron microscopy. *Journal of Neuroscience.* **26** (47), 12101-12103. (2006).

22. Jesior, J. C. Use of low-angle diamond knives leads to improved ultrastructural preservation of ultrathin sections. *Scanning Microscopy Supplement.* **3**, 147-152; discussion 152-143 (1989).

23. Studer, D., Gnaegi, H. Minimal compression of ultrathin sections with use of an oscillating diamond knife. *Journal of Microscopy.* **197** (Pt 1), 94-100 (2000).

24. Gay, H., Anderson, T. F. Serial sections for electron microscopy. *Science.* **120** (3130), 1071-1073 (1954).

25. Bernhard, W., Rouiller, C. Close topographical relationship between mitochondria and ergastoplasm of liver cells in a definite phase of cellular activity. *The Journal of Biophysical and Biochemical Cytology.* **2** (4 Suppl), 73-78 (1956).

26. Palade, G. E. An electron microscope study of the mitochondrial structure. *The Journal of Histochemistry & Cytochemistry.* **1** (4), 188-211 (1953).

27. Wu, H., Carvalho, P., Voeltz, G. K. Here, there, and everywhere: The importance of ER membrane contact sites. *Science.* **361** (6401), eaan5835 (2018).

28. Vance, J. E. Inter-organelle membrane contact sites: implications for lipid metabolism. *Biology Direct.* **15** (1), 24 (2020).

29. Stefan, C. J. Endoplasmic reticulum-plasma membrane contacts: Principals of phosphoinositide and calcium signaling. *Current Opinion in Cell Biology.* **63**, 125-134 (2020).

30. Zaman, M. F., Nenadic, A., Radojicic, A., Rosado, A., Beh, C. T. Sticking with it: ER-PM membrane contact sites as a coordinating nexus for regulating lipids and proteins at the cell cortex. *Frontiers in Cell and Developmental Biology.* **8**, 675 (2020).

31. van Vliet, A. R., Sassano, M. L., Agostinis, P. The unfolded protein response and membrane contact sites: tethering as a matter of life and death? *Contact.* **1**, 1-15 (2018).

32. Cohen, S., Valm, A. M., Lippincott-Schwartz, J. Interacting organelles. *Current Opinion in Cell Biology.* **53**, 84-91 (2018).

33. Hariri, H. et al. Lipid droplet biogenesis is spatially coordinated at ER-vacuole contacts under nutritional stress. *EMBO Reports.* **19** (1), 57-72 (2018).

34. Stefan, C. J., Trimble, W. S., Grinstein, S., Drin, G. Membrane dynamics and organelle biogenesis-lipid pipelines and vesicular carriers. *BMC Biology.* **15** (1), 102 (2017).

35. Eisenberg-Bord, M., Shai, N., Schuldiner, M., Bohnert, M. A tether is a tether is a tether: tethering at membrane contact sites. *Developmental Cell.* **39** (4), 395-409 (2016).

36. Scorrano, L., De Matteis, M. A., Emr, S., Giordano, F. Coming together to define membrane contact sites. *Nature Communications.* **10** (1), 1287 (2019).

37. Lak, B., Li, S., Belevich, I., Sree, S. Specific subdomain localization of ER resident proteins and membrane contact sites resolved by electron microscopy. *European Journal of Cell Biology.* **100** (7), 151180 (2021).

38. Collado, J., Kalemanov, M., Campelo, F., Bourgoint, C. Tricalbin-mediated contact sites control ER curvature to maintain plasma membrane integrity. *Developmental Cell.* **51** (4), 476-487 e477 (2019).

39. West, M., Zurek, N., Hoenger, A., Voeltz, G. K. A 3D analysis of yeast ER structure reveals how ER domains are organized by membrane curvature. *Journal of Cell Biology.* **193** (2), 333-346 (2011).

40. Ilacqua, N., Anastasia, I., Raimondi, A., Lemieux, P. A three-organelle complex made by wrappER contacts with peroxisomes and mitochondria responds to liver lipid flux

changes. *Journal of Cell Science.* **135** (5), jcs259091 (2022).

41. Cardona, A., Saalfeld, S., Schindelin, J., Arganda-Carreras, I. TrakEM2 software for neural circuit reconstruction. *PLoS One.* **7** (6), e38011 (2012).

42. Stalling, D., Westerhoff, M., Hege, H.-C. Amira: A highly interactive system for visual data analysis. *The Visualization Handbook.* **38**, 749-767 (2005).

43. Hsieh, T. S., Chen, Y. J., Chang, C. L., Lee, W. R., Liou, J. Cortical actin contributes to spatial organization of ER-PM junctions. *Molecular Biology of the Cell.* **28** (23), 3171-3180 (2017).

44. Anastasia, I., Ilacqua, N., Raimondi, A., Lemieux, P. Mitochondria-rough-ER contacts in the liver regulate systemic lipid homeostasis. *Cell Reports.* **34** (11), 108873 (2021).

45. Cattin, A. L., Burden, J. J., Van Emmenis, L., Mackenzie, F. E. Macrophage-Induced Blood Vessels Guide Schwann Cell-Mediated Regeneration of Peripheral Nerves. *Cell.* **162** (5), 1127-1139 (2015).

46. Lopes-da-Silva, M. et al. A GBF1-dependent mechanism for environmentally responsive regulation of ER-Golgi transport. *Developmental Cell.* **49** (5), 786-801 e786 (2019).

47. Banushi, B., Forneris, F., Straatman-Iwanowska, A., Strange, A. Regulation of post-Golgi LH3 trafficking is essential for collagen homeostasis. *Nature Communications.* **7**, 12111 (2016).

48. Rey, S. A. et al. Ultrastructural and functional fate of recycled vesicles in hippocampal synapses. *Nature Communications.* **6**, 8043 (2015).

49. Belicova, L., Repnik, U., Delpierre, J., Gralinska, E. Anisotropic expansion of hepatocyte lumina enforced by apical bulkheads. *Journal of Cell Biology.* **220** (10), e202103003 (2021).

50. Kizilyaprak, C., Daraspe, J., Humbel, B. M. Focused ion beam scanning electron microscopy in biology. *Journal of Microscopy.* **254** (3), 109-114 (2014).

51. Xu, C. S., Hayworth, K. J., Lu, Z., Grob, P. Enhanced FIB-SEM systems for large-volume 3D imaging. *Elife.* **6**, 1-36 (2017).

52. Parlakgül, G., Arruda, A.P., Cagampan, E., Pang, S. High resolution 3D imaging of liver reveals a central role for subcellular architectural organization in metabolism. *bioRxiv.* https://www.biorxiv.org/content/biorxiv/early/2020/11/18/2020.11.18.387803.full.pdf (2020).

53. Guerin, C. J., Kremer, A., Borghgraef, P., Lippens, S. Targeted studies using serial block face and focused ion beam scan electron microscopy. *The Journal of Visualized Experiments: JoVE.* (150), doi. 10.3791/59480 (2019).

54. Kremer, A. et al. A workflow for 3D-CLEM investigating liver tissue. *Journal of Microscopy.* **281** (3), 231-242 (2021).

55. Hayat, M. *Principles and techniques of electron microscopy: biological applications.* Cambridge University Press (2000).

56. Wisse, E., Braet, F., Duimel, H., Vreuls, C. Fixation methods for electron microscopy of human and other liver. *World Journal of Gastroenterology.* **16** (23), 2851-2866 (2010).

57. Hanley, J., Dhar, D. K., Mazzacuva, F., Fiadeiro, R. Vps33b is crucial for structural and functional hepatocyte polarity. *Journal of Hepatology.* **66** (5), 1001-1011 (2017).

58. Deerinck, T. J., Bushong, E. A., Thor, A., Ellisman, M. H. NCMIR methods for 3D EM: a new protocol for preparation of biological specimens for serial block face scanning electron microscopy. *Microscopy.* **1**, 6-8 (2010).

59. Miranda, K., Girard-Dias, W., Attias, M., de Souza, W., Ramos, I. Three dimensional reconstruction by electron microscopy in the life sciences: An introduction for cell and tissue biologists. *Molecular Reproduction and Development.* **82** (7-8), 530-547 (2015).

60. Yamaguchi, M., Chibana, H. A method for obtaining serial ultrathin sections of microorganisms in transmission electron microscopy. *The Journal of Visualized Experiments: JoVE.* (131), 56235 (2018).

61. Hall, D. H., Hartwieg, E., Nguyen, K. C. Modern electron microscopy methods for C. elegans. *Methods in Cell Biology.* **107**, 93-149 (2012).

62. Hagler, H. K. Ultramicrotomy for biological electron microscopy. *Methods in Molecular Biology.* **369**, 67-96 (2007).

63. Arganda-Carreras, I. et al. Consistent and elastic registration of histological sections using vector-spline regularization. In *Computer vision approaches to medical image analysis.* Beichel, R. R., Sonka, M. (Eds), CVAMIA 2006, Lecture Notes in Computer Science, Springer Berlin Heidelberg, Berlin, Heidelberg, **4241**, 85-95 (2006).

64. Belevich, I., Joensuu, M., Kumar, D., Vihinen, H., Jokitalo, E. Microscopy image browser: a platform for segmentation and analysis of multidimensional datasets. *PLoS Biology.* **14** (1), e1002340 (2016).

65. Fiala, J. C. Reconstruct: a free editor for serial section microscopy. *Journal of Microscopy.* **218** (Pt 1), 52-61 (2005).

66. Kremer, J. R., Mastronarde, D. N., McIntosh, J. R. Computer visualization of three-dimensional image data using IMOD. *Journal of Structural Biology.* **116** (1), 71-76 (1996).

67. Iudin, A., Korir, P. K., Salavert-Torres, J., Kleywegt, G. J., Patwardhan, A. EMPIAR: a public archive for raw electron microscopy image data. *Nature Methods.* **13** (5), 387-388 (2016).

68. Xu, C. S., Pang, S., Shtengel, G., Muller, A. An open-access volume electron microscopy atlas of whole cells and tissues. *Nature.* **599** (7883), 147-151 (2021).

69. Karabag, C. et al. Semantic segmentation of HeLa cells: An objective comparison between one traditional algorithm and four deep-learning architectures. *PLoS One.* **15** (10), e0230605 (2020).

70. Heinrich, L., Bennett, D., Ackerman, D., Park, W. Whole-cell organelle segmentation in volume electron microscopy. *Nature.* **599** (7883), 141-146 (2021).

71. Kim, J. S., Greene, M. J., Zlateski, A., Lee, K. Space-time wiring specificity supports direction selectivity in the retina. *Nature.* **509** (7500), 331-336 (2014).

72. Spiers, H., Songhurst, H., Nightingale, L., de Folter, J. Deep learning for automatic segmentation of the nuclear envelope in electron microscopy data, trained

with volunteer segmentations. *Traffic.* **22** (7), 240-253 (2021).

73. Hasan, N. M., Gupta, A., Polishchuk, E., Yu, C. H. Molecular events initiating exit of a copper-transporting ATPase ATP7B from the trans-Golgi network. *The Journal of Biological Chemistry.* **287** (43), 36041-36050 (2012).

74. Stoeck, I. K., Lee, J. Y., Tabata, K., Romero-Brey, I. Hepatitis C virus replication depends on endosomal cholesterol homeostasis. *The Journal of Virology.* **92** (1), e01196-17 (2018).

75. Ma, X., Qian, H., Chen, A., Ni, H. M., Ding, W. X. Perspectives on mitochondria-ER and mitochondria-lipid droplet contact in hepatocytes and hepatic lipid metabolism. *Cells.* **10** (9), 2273 (2021).